 ISSN 0267-8179. DOI: 10.1002/jqs.2998

JQS Journal of Quaternary Science QRA Quaternary Research Association

Re-evaluation of MIS 3 glaciation using cosmogenic radionuclide and single grain luminescence ages, Kanas Valley, Chinese Altai

NATACHA GRIBENSKI,[1,2]* KRISTER N. JANSSON,[1] FRANK PREUSSER,[3] JONATHAN M. HARBOR,[1,4] ARJEN P. STROEVEN,[1] MAREIKE TRAUERSTEIN,[5] ROBIN BLOMDIN,[1] JAKOB HEYMAN,[6] MARC W. CAFFEE,[4,7] NATHANIEL A. LIFTON[4,7] and WEI ZHANG[8]

[1]Geomorphology and Glaciology, Department of Physical Geography and Bolin Centre for Climate Research, Stockholm University, Sweden
[2]Leibniz Institute for Applied Geophysics, Hannover, Germany
[3]Institute of Earth and Environmental Sciences, University of Freiburg, Germany
[4]Department of Earth, Atmospheric, and Planetary Sciences, Purdue University, IN, USA
[5]Institute of Geography, University of Bern, Switzerland
[6]Department of Earth Sciences, University of Gothenburg, Sweden
[7]Department of Physics and Astronomy, Purdue University, IN, USA
[8]College of Urban and Environmental Sciences, Liaoning Normal University, China

Received 20 April 2017; Revised 1 September 2017; Accepted 15 September 2017

ABSTRACT: Previous investigations observed a period of major glacial advances in Central Asia during marine oxygen isotope stage (MIS) 3 (57–29 ka), out of phase with global ice volume records. We have re-examined the Kanas moraine complex in the Altai Mountains of Central Asia, where an MIS 3 glaciation had been previously inferred. New and consistent cosmogenic exposure and single-grain luminescence ages indicate that the Kanas complex was formed during MIS 2 (29–12 ka), which brings its timing in line with the global ice volume record. We also identified a lateral moraine from a more extensive ice extent that dates to late MIS 5/MIS 4. To place our results in a wider contextual framework, we review the chronologies of another 26 proposed major MIS 3 glacial advances in Central Asia. For most of these sites, we find that the chronological data do not provide an unequivocal case for MIS 3 glaciation. Copyright © 2017 John Wiley & Sons, Ltd.

KEYWORDS: Central Asia; cosmogenic exposure dating; glaciation; MIS 3; OSL dating.

Introduction

Detailed geomorphic and chronological reconstructions of former glaciations offer a means of understanding variations in past atmospheric circulation and testing the validity of ice sheet and climate models (e.g. Kuhlemann *et al.*, 2008; Seguinot *et al.*, 2016). On a global scale, marine records indicate that Last Glacial Maximum (LGM) ice volumes occurred at Marine Isotope Stage (MIS) 2, between 29 and 19 ka (Lisiecki and Raymo, 2005; Lambeck *et al.*, 2014). While there is widespread empirical evidence that ice sheets and alpine glaciers in most formerly glaciated areas experienced major MIS 2 expansion (Hughes *et al.*, 2013), some studies indicate that maximum ice extents were attained at significantly earlier times in many mountain areas (Ehlers *et al.*, 2011; Hughes *et al.*, 2013). Particularly intriguing examples are glaciers from the Himalayan, Tibetan and Central Asian mountains, for which several paleoglacial reconstructions indicate rather limited MIS 2 ice extent and major glacial advances during MIS 3 (57–29 ka; e.g. Koppes *et al.*, 2008; Heyman, 2014; Owen and Dortch, 2014), a period of relative global warmth (van Meerbeeck *et al.*, 2009). This regional asynchronicity has been explained by increased moisture supply during MIS 3 and arid conditions during MIS 2 (e.g. Owen *et al.*, 2002; Zhao *et al.*, 2013; Li *et al.*, 2014).

Glaciation patterns at the regional or global scale and their interpretation in terms of paleo-atmospheric circulation are highly dependent on the accurate chronologies of local glacial extent. The most unambiguous approach for constraining the timing of a former glacial extent is to directly date landforms and deposits associated with ice margins (e.g. moraines). The timing of glacial deposition is typically constrained by cosmogenic nuclide exposure dating of boulders from moraines crests, or by dating ice marginal sediments using optically stimulated luminescence (OSL) or, more rarely, electron spin resonance (ESR) techniques. Obtaining accurate glacial chronologies is a challenge because geomorphological processes inherent to glacial settings often complicate interpretation of measured parameters serving as proxies for age (Fuchs and Owen, 2008; Balco, 2011; Heyman *et al.*, 2011; Fu *et al.*, 2013).

A case in point is the glacial chronology of Kanas Valley in the Chinese Altai Mountains, Central Asia (Fig. 1A,B). Previous studies identified at least four sets of moraines along this valley, which were dated using OSL and ESR techniques (Zhao *et al.*, 2013, and references therein; Yang *et al.*, 2017). In particular, an extensive well-preserved moraine complex at ~1400 m a.s.l., located ~80 km from the valley headwaters at the outlet of Lake Kanas (Fig. 1; third set in Zhao *et al.*, 2013), has been divided into three subsets based primarily on moraine ridge density, height and slope criteria. Using OSL dating, these three subsets were related to glacial stages during MIS 2 (~28 ka), mid-MIS 3 (~38–52 ka) and early MIS 3 or MIS 4 (~50 or ~73 ka; Xu *et al.*, 2009; Zhao *et al.*, 2013), respectively. In addition, Zhao *et al.* (2013) propose a larger MIS 6 glaciation, based on weathered lateral moraine benches found discontinuously at about 200 m above the Kanas River from the Lake Kanas outlet to ~ 20 km downstream (fourth set in their study), and using ESR ages from Xu (2010). Alternatively, Yang *et al.* (2017) suggest an MIS 5 age for this moraine set, based on OSL ages from an

*Correspondence: N. Gribenski, Geomorphology and Glaciology, as above.
E-mail: natacha.gribenski@natgeo.su.se

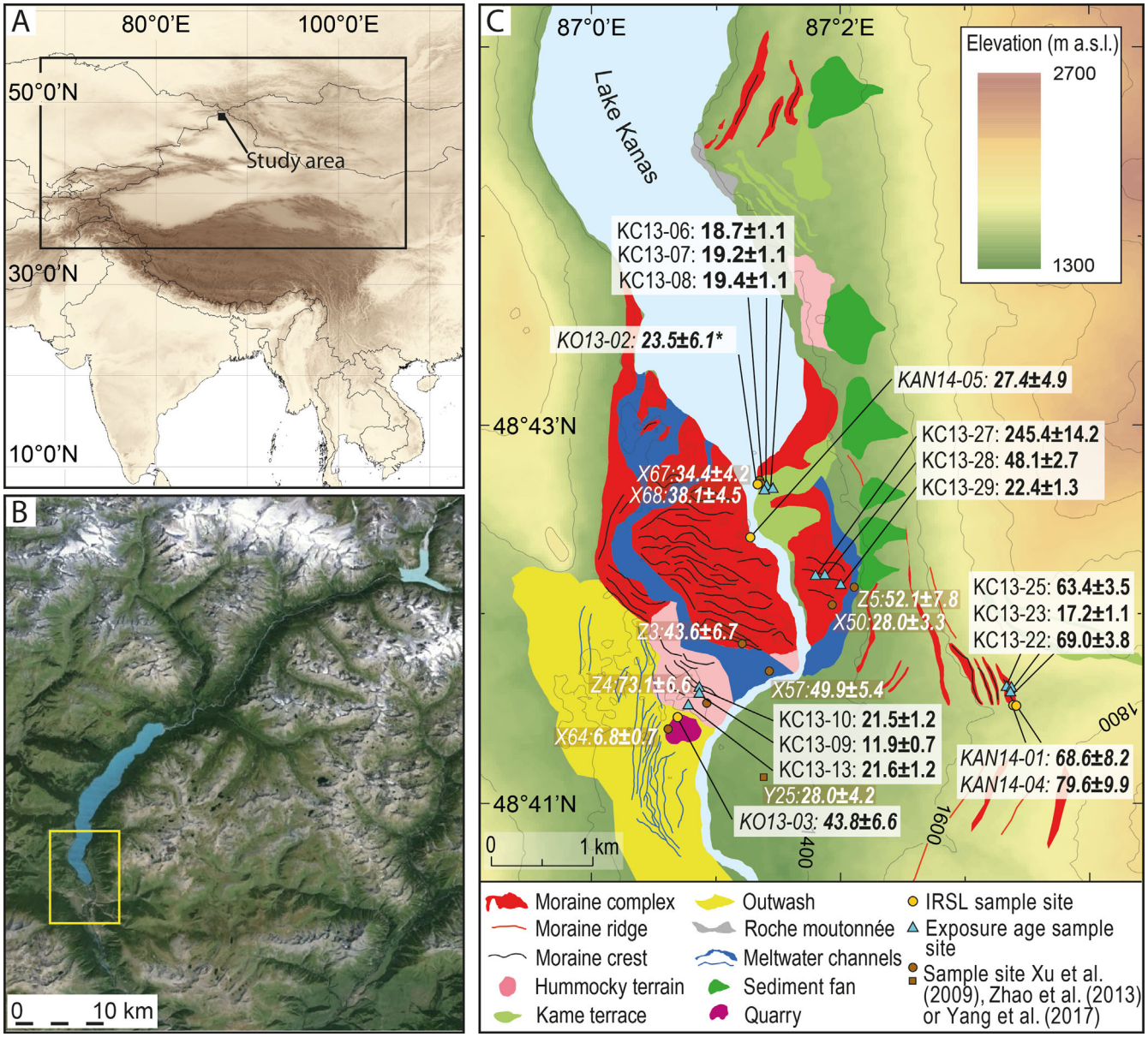

Figure 1. (A) Study area in north-western China (arrow) in Central Asia (black box; Fig. 5B map extent). (B) Lower Kanas Valley and the study area at the outlet of Lake Kanas (yellow box, panel C). GoogleEarth©. (C) Geomorphological evidence for former glacial extents in the study area; Labeled in black are ^{10}Be cosmogenic nuclide exposure and single grain infra-red luminescence (IRSL, in italic) sample locations and ages produced in this study. In bold white are OSL ages (circle brown symbol) and one ESR age (square brown symbol) produced in previous studies (Xu *et al.*, 2009; Zhao *et al.*, 2013; Yang *et al.*, 2017). The IRSL age denoted with an asterisk was obtained from the same section sampled by Xu *et al.* (2009) for which they obtained ages of 34.4 ± 4.2 and 38.1 ± 4.5 ka. The location of samples from previous studies is based on published coordinates and photos.

older glacio-fluvial terrace. All the authors also indicate the presence of erratics above 1850 m a.s.l., and suggest these are traces of an even larger and older glaciation. At the present time, no chronological data exists for this event. We present here a revised glacial chronology of Kanas Valley using cosmogenic nuclide exposure dating of boulders in conjunction with OSL dating of sediments associated with moraine landforms in the Lake Kanas outlet area. To place our results in a better contextual framework, we review the data supporting major MIS 3 glaciation in other parts of the Central Asian mountains.

Methods

Geomorphological mapping

Detailed geomorphological mapping was conducted in the Lake Kanas outlet area, with a focus on glacial landforms to constrain former glacial extents. Moraines, hummocky terrain, kame terraces, outwash deposits and meltwater channels were identified using the criteria summarized in Table 1. Satellite imagery (Google Earth) and digital elevation models (ASTER and SRTM) were used for preliminary 'on screen' mapping; geomorphological and sedimentological field-based observations were combined with the remote sensing observations.

Cosmogenic exposure dating

Twelve samples for cosmogenic exposure dating were collected in 2013 from the upper surface of large granitic boulders (60–155 cm high) located on the top of moraines (Fig.1C and Supporting Infirmation, Fig. S1). Each sample was crushed and sieved to 250–500 μm. Quartz was isolated following procedures modified after Kohl and Nishiizumi (1992). Purity was checked through trace element analysis

Table 1. Recognition criteria of landforms and deposits mapped in Kanas Valley.

Landform	Geomorphological and sedimentological descriptive criteria*	Main sediment association*
Marginal moraine (complex, ridge, crest)	Prominent deposits of varying width, from single to multiple (complex) ridges, with more or less well-defined crests, which extend across valley floors and/or along valley sides. Linear, curved, sinuous or saw-toothed in planform.	May include a variety of sediment facies, from till to debris flow. May include glaciofluvial units.
Hummocky terrain	Protruding deposit with irregular shape in planform and with an irregular gentle topography of alternating hills (or crests) and depressions.	May include a variety of sediment facies, from till to debris flow and glaciofluvial deposits.
Roches moutonnées	Bare bedrock features, with stoss- and lee-side topography. Glacial striations on rock surface.	–
Kame terrace	Flat to gentle surface, with potential smooth slope, often found in association with moraines.	Mainly composed of bedded sand and gravel units (glaciofluvial).
Outwash	Flat to very gently sloping plain, often downstream marginal moraines.	Layered and sorted sand-to-cobble deposit (glaciofluvial)
Meltwater channel	Linear depression on bedrock or sediment. Can be parallel to, or cross-cut, the valley slope. Can also be parallel to, or cross-cut, moraine deposits.	–
Sediment fan	Prominent deposit with a fan shape in planform located at the foot of the valley slope. Non-glacial deposit.	Poorly sorted and angular clast-dominated deposit (if mainly due to physical weathering; colluvial fan) to more stratified and sorted deposit (if streams involved in sediment transport along slopes; alluvial fan)

*Criteria mainly based on Heyman et al. (2008), Benn and Evans (2010), Gribenski *et al.* (2016), Blomdin *et al.* (2016a).

using inductively coupled plasma optical emission spectrometry. Samples were then dissolved in HF and HNO_3, and spiked with a Be carrier. Standard anion and cation exchange column procedures were used to separate ^{10}Be and ^{26}Al (e.g. Ochs and Ivy-Ochs, 1997). Resulting Be and Al oxides were mixed with Nb and Ag powders, respectively, and filled into target holders (cathodes). Final concentrations of ^{10}Be (all samples) and ^{26}Al (nine samples) were measured by accelerator mass spectrometry (AMS) at PRIME Lab (Sharma *et al.*, 2000). The data are presented in Table 2. Ages were calculated using the expage-201611 calculator (expage.github.io/calculator). This calculator is based on the CRONUS calculator, version 2 (Balco *et al.*, 2008), but uses the nuclide-specific ^{10}Be and ^{26}Al LSD production rate scaling including the LSD geomagnetic framework (Lifton *et al.*, 2014b) and global average reference production rates based on calibration sites with well-clustered data published between 2009 and 2016 (^{10}Be: 3.98 ± 0.21 atoms g^{-1} year^{-1}; ^{26}Al: 28.41 ± 1.89 atoms g^{-1} year^{-1}). The site atmospheric pressure is calculated using the 'std' ERA-40 interpolation (ERA40atm.m; Lifton *et al.*, 2014b). Corrections for topographic shielding were included in the calculation; shielding effects by snow and vegetation were neglected. Likewise, ages were calculated assuming zero erosion because no reliable long-term boulder surface erosion rates are available in the area. For an erosion rate of 3 mm ka^{-1}, which corresponds to the maximum erosion rate value used by others in Central Asia (e.g. Koppes *et al.*, 2008; Rother *et al.*, 2014), we would expect a maximum increase of ~5% for ages ~20 ka, of ~8% for ages ~30 ka and of ~17% for ages ~60 ka (e.g. Blomdin *et al.*, 2016b).

Optically stimulated luminescence dating

Four samples for OSL dating were collected in opaque tubes from sediments embedded within moraines, and an additional non-morainic sample was collected from a glaciofluvial unit in a quarry directly downstream of the Kanas moraine complex (Figs 1C and S2; Table S1) during 2013 and 2014. The sediments sampled in the moraines are interpreted to represent low-energy glaciofluvial and glaciolimnic (ponding) facies in ice marginal positions. Coarse-grain (200–250 μm) and fine-grain (<63 μm) fractions were isolated using wet sieving. Following HCl and H_2O_2 pre-treatment to remove carbonates and organics, K-feldspar grains were isolated from the coarse fraction using density separation (sodium heteropolytungstate solution, density <2.58 g cm^{-3}). Polymineral fine grains (4–11 μm) were isolated from the <63 μm fraction by settling in Atterberg cylinders according to the principle of Stokes' law. Because preliminary luminescence signal measurements indicated the absence of a suitable quartz blue OSL signal, all the measurements were performed on the feldspar fraction, using the infra-red signal measured at 50 °C ($IRSL_{50}$). The $IRSL_{50}$ signal was selected based on its higher bleaching properties compared to more stable but less bleachable IRSL signal measured at higher temperatures (Kars *et al.*, 2014). A modified SAR protocol was applied to determine the IRSL equivalent doses (D_e) (Wallinga *et al.*, 2000), using a constant preheat and cut heat (60 s at 260 °C; Blair *et al.*, 2005). D_e measurements for final age calculation were carried out at the single grain scale (200–250 μm), using a Risø DA-20 TL/OSL single grain reader system (Bøtter-Jensen *et al.*, 2003). Additional D_e measurements were conducted for comparison on the fine fraction (4–11 μm) laid as a coating on a 10-mm aliquot, using a Freiberg Instruments Lexsyg Research reader (Richter *et al.*, 2013). For data analysis, the IRSL signal was background corrected (first 0.5 s minus a background averaged over the last 2 s for single grain measurements; first 25 s minus a background averaged over the last 100 s for fine multi-grain measurements). Dose–response curves were reconstructed using an exponential fitting, and an instrumental uncertainty of 2.5% was incorporated for D_e calculation. Grains/aliquots were accepted if the signal was >3σ above the background, the recuperation signal was <15% of the natural signal, the recycling ratio was within 15% of unity

Table 2. Details of ^{10}Be and ^{26}Al cosmogenic nuclide samples, analysis and corresponding surface exposure ages.

Sample	Feature sampled	Location (°N/°E)	Altitude (m a.s.l.)	Thickness (cm)	Shielding	[^{10}Be] (10^5at g−1)	[^{26}Al] (10^5at g^{-1})	^{10}Be ages (ka)	Ext. unc.	Int. unc.	^{26}Al ages (ka)	Ext. unc.	Int. unc.
KC13-06	Kanas moraine complex	48.7111/87.0231	1386	1.5	0.99786	2.387 ± 0.055	17.921 ± 0.497	18.7	1.1	0.4	20.0	1.5	0.6
KC13-07		48.7108/87.0232	1384	3.0	0.99786	2.418 ± 0.061	17.999 ± 0.516	19.2	1.1	0.5	20.3	1.5	0.6
KC13-08		48.7110/87.0239	1387	2.5	0.99786	2.466 ± 0.053	17.391 ± 0.519	19.4	1.1	0.4	19.5	1.4	0.6
KC13-09		48.6931/87.0143	1387	2.0	0.99804	1.498 ± 0.038	10.742 ± 0.329	11.9	0.7	0.3	12.2	0.9	0.4
KC13-10		48.6934/87.0143	1388	2.5	0.99804	2.746 ± 0.060	19.513 ± 0.562	21.5	1.2	0.5	21.8	1.6	0.6
KC13-13		48.6919/87.0134	1386	2.0	0.99775	2.762 ± 0.054	18.300 ± 0.498	21.6	1.2	0.4	20.5	1.5	0.6
KC13-27		48.7032/87.0300	1397	1.5	0.99664	30.960 ± 0.403	195.422 ± 3.520	245.4	14.2	3.4	230.8	17.9	4.7
KC13-28		48.7031/87.0311	1406	4.0	0.99571	6.240 ± 0.110	43.997 ± 1.080	48.1	2.7	0.9	48.6	3.5	1.2
KC13-29		48.7024/87.0332	1411	1.0	0.99457	2.939 ± 0.057	19.910 ± 0.594	22.4	1.3	0.4	21.6	1.6	0.7
KC13-22	Outer lateral moraine ridge	48.6930/87.0562	1654	2.0	0.99730	11.128 ± 0.127	–	69.0	3.8	0.8	–	–	–
KC13-23		48.6933/87.0562	1659	2.5	0.99730	2.723 ± 0.089	–	17.2	1.1	0.6	–	–	–
KC13-25		48.6939/87.0555	1656	2.0	0.99667	10.238 ± 0.138	–	63.4	3.5	0.9	–	–	–

Samples were measured using the ^{10}Be isotope ratio standardization 07KNSTD (Nishiizumi *et al.*, 2007) and the ^{26}Al isotope ratio standardization KNSTD (Nishiizumi, 2004). Final ^{10}Be and ^{26}Al concentrations include measured blank corrections (correcting value based on averaged nuclide concentrations of the blanks processed during the AMS measurements of the samples) that corresponds to <0.4% for both ^{10}Be and ^{26}Al measurements, except in the case KC13-23, where it corresponds to ~0.9% for ^{10}Be measurements. The adopted rock density is 2.65 $^{-}$ g cm^{-3}.

and if the recovered D_e was $<2D_0$ of the exponential curve fit (Wintle and Murray, 2006). The reliability of the protocol was tested by conducting dose recovery experiments on two samples (KO13-03 and 01) previously exposed to a Sunlux Ambience UV lamp for 48 h. For both grain fractions, we obtained dose recovery ratio within 10% of unity (with overdispersion below 10%). Final equivalent doses used for final age determination were calculated using the Central Age Model (CAM) or, when partial bleaching of the sample was inferred, using the Minimum Age Model (MAM; Galbraith *et al.*, 1999). In the latter case, a σ_b value of 0.3 (overdispersion expected for a well-bleached sample) was adopted, based on single grain IRSL overdispersion values reported for proglacial deposits interpreted to have been well bleached (Gaar *et al.*, 2013).

Laboratory fading rate (*g*-value) measurements were performed on representative samples (KAN14-01 and 5) from the two main sampling sites, following the procedure of Auclair *et al.* (2003), and using the same measurement parameters as for D_e determination. Due to poor counting statistics, fading tests for coarse K-feldspar grains were performed using large aliquots (~6 mm, three aliquots per sample) to produce a high-magnitude signal and allow a better detection of small signal variation. Fading measurements from polymineral fine-grain fractions produced inconsistent results with unreasonably high uncertainties (>100%) and were therefore disregarded. Final averaged *g*-value obtained for KAN14-05 was also applied to KAN13-02, and the *g*-value obtained for KAN14-01 was used for KAN14-04 and KAN13-03, based on similar sedimentology characteristic and sample locations. All final ages have been corrected for anomalous fading following the fading correction procedure of Huntley and Lamothe (2001).

External dose rates were determined based on high-resolution gamma spectrometry measurements of bulk material collected from the sampling point and assuming an internal K-content of 12.5 ± 0.5% (Huntley and Baril, 1997; Trauerstein *et al.*, 2014; Table 3) for final dose rate calculations. Because no clear relationship could be observed between single-grain D_e values and signal intensity in a sample interpreted as well bleached before deposition (KAN14-04 discussed in 'Kanas valley glacial chronology'; Fig. S3), this suggests that there is no major influence of the grain-to-grain variability of the internal K-content (Smedley and Pearce, 2016). Based on direct water content measurements and previous water content values from this study area (cf. Xu *et al.*, 2009; Zhao *et al.*, 2013), we attributed water content values ranging from 7 to 15% to the measured samples (Table 3) for final determination of the dose rate.

Re-evaluation of proposed MIS 3 glacial advances

MIS 3 glaciations have been proposed in the Pamir, the Tian Shan, the Kunlun Shan, the Altai and the Khangai mountains. We review datasets of cosmogenic, OSL and ESR ages that have been used to infer or suggest MIS 3 glacial advances in these areas. Only age constraints from direct dating of moraines are considered. These data were evaluated against specific criteria for the three dating methods. For all dating methods, we required multiple sample measurements to allow for some control of age consistency; single-sample age determinations were discarded (Dortch *et al.*, 2013; Small *et al.*, 2017). We recalculated all ^{10}Be exposure ages using the same approach and calculator (expage-201611) as described for the Kanas Valley samples age calculation (see 'Cosmogenic exposure dating'), for consistency. Inheritance of cosmogenic nuclides and post-depositional processes can alter moraine boulder exposure ages producing scatter, which in turn hampers a robust determination of a moraine

Table 3. Details of luminescence samples and corresponding ages from the Kanas Lake outlet area.

				Dose rate							Single coarse grain			Multi-fine grains
Sample	Feature sampled	Location (°N/°E)	Alt. (m a.s.l.)	Depth (cm)	^{40}K (Bq kg^{-1})	U (Bq kg^{-1})	Th (Bq kg^{-1})	Water content (%)	Total dose rate (Gy ka^{-1}) – coarse grains	Total dose rate (Gy ka^{-1}) – fine grains	n^*	OD (%)	CAM age (ka)†	MAM age (ka)†	CAM age (ka)†
KO13-02	Kanas moraine complex	48.7114/87.0226	1383	200	608.7 ± 49.4	32.0 ± 3.5	44.0 ± 2.9	7 ± 3	4.09 ± 0.31	4.26 ± 0.55	68	46.5	45.5 ± 5.5	**23.5 ± 6.1**	62.3 ± 9.7
KAN14-05		48.7068/87.0213	1382	80	547.2 ± 9.6	30.0 ± 0.6	41.0 ± 1.9	7 ± 3	3.86 ± 0.20	3.97 ± 0.38	72	42.8	43.0 ± 4.7	**27.4 ± 4.9**	62.6 ± 9.7
KO13-03	Outwash	48.6911/87.0116	1373	300	692.2 ± 55.6	22.2 ± 3.7	33.4 ± 2.0	10 ± 5	3.85 ± 0.36	–	63	31.1	**43.8 ± 6.6**	–	–
KAN14-01	Outer lateral moraine ridge	48.6920/87.0567	1627	200	662.8 ± 9.6	31.1 ± 0.7	35.6 ± 2.0	15 ± 5	3.85 ± 0.23	3.85 ± 0.38	66	13.2	**68.6 ± 8.2**	–	68.9 ± 10.5
KAN14-04		48.6922/87.0569	1616	200	634.7 ± 6.2	27.1 ± 0.9	34.7 ± 1.0	15 ± 5	3.70 ± 0.22	3.65 ± 0.35	20	9.4	**79.6 ± 9.9**	–	60.4 ± 9.5

*Number of grains accepted.
†Fading corrections have been applied to all the reported ages (using averaged measured fading rates, *g*-values, of 1.6 ± 0.8% for KO13-02 and KAN14-05; of 2.9 ± 0.9% for KO13-03, KAN14-01 and KAN14-04). Ages in bold are the ages used for final interpretation.

deposition time (Balco, 2011). This is particularly true for glacial deposits from Central Asia older than MIS 2 (Heyman, 2014; Blomdin *et al.*, 2016b). For consideration, our criteria require at least (i) three individual samples per moraine set with (ii) an exposure age standard deviation of ≤15% of the mean exposure age (coefficient of variation $\sigma/\mu \leq 15\%$; Blomdin *et al.*, 2016b). An additional criterion is that no more than one-third of the initial number of samples are outliers (still requiring a minimum of three individual samples after outlier rejection) to permit for a minor portion of samples being affected by significant prior or incomplete exposure. The minimum number of three clustered ages (after outlier rejection) is based on the low probability that three similar ages yield an incorrect age range (Dortch *et al.*, 2013). Final groups of cosmogenic exposure ages fulfilling the clustering criterion ($\sigma/\mu \leq 15\%$) may include samples affected to some degree by prior and/or incomplete exposure, but a reliable glaciation timing with reasonable uncertainty may still be inferred. Our statistical criteria are somewhat arbitrary but it is rigorous enough to eliminate ages based on highly scattered or insufficient data and at the same time it is not so rigid as to preclude an ample data set. Although our approach disregards original field observations, it allows for an objective analysis with consistent criteria for multiple studies and without subjective decisions for each site.

A common problem for OSL dating of glacial and glaciofluvial sediments is the risk of partial bleaching, which corresponds to the incomplete resetting of the luminescence signal within the grains at deposition due to limited light exposure during their transport. This may lead to significant age overestimation if undetected (Duller, 2006; Fuchs and Owen, 2008). For reliable OSL ages from glacial environments we require thorough investigation of potential partial bleaching, such as small aliquot/single grain D_e distribution analysis, or signal comparison for different aliquot size or wavelength stimulation (Fuchs and Owen, 2008; Hughes *et al.*, 2016; Small *et al.*, 2017). In the absence of in-depth partial bleaching examination, the robustness of derived OSL ages remains uncertain and would need additional supporting chronological data to be validated.

Resetting of the ESR signal [germanium (Ge) paramagnetic centre] is even more problematic in glacial settings, as it requires extensive light exposure (up to several days), which is unlikely during glacial sediment transport. Likewise, subglacial grinding processes have been shown to be of limited efficiency in resetting the ESR signal (Yi *et al.*, 2016). For ESR ages to be accepted as reliable, we would require data that with reasonable certainty indicate complete resetting of the ESR signal or for which we can quantify the residual dose at the time of deposition. There are no routine techniques to quantify the residual dose or to check if the signal has been properly reset. Consistent independent ages are required to regard ESR chronologies as reliable or a need for residual dose estimates based on measurements from local modern analogs that are integrated in ESR age calculations.

Results and revised Kanas Valley glacial chronology

Geomorphological setting of the Kanas Lake outlet area

Two main glacial landform associations are clearly identified in the Lake Kanas outlet area (Fig. 1C). A stratigraphically younger moraine complex extends over ~4 km^2 across the Kanas Valley, at the edge of Lake Kanas. The moraine complex includes a series of moraine ridges associated with kame terraces that grade outward into hummocky terrain. An

outwash plain spreads downstream from the Kanas complex. The moraine ridges may reflect multiple glacial advances/stillstands of the ice margin, accompanied by the formation of kame terraces due to the trapping of glacier meltwater in the local topography. The distal hummocky terrain probably results from ice decay moraine degradation, common in alpine settings (Benn and Owen, 2002), and is therefore not indicative of a separate glacial event. Overall, there is no distinctive geomorphological evidence to support a previous subdivision of the Kanas complex into three subsets associated with distinct glaciations (Xu *et al.*, 2009; Zhao *et al.*, 2013). More discrete moraine ridges and remnants of kame terraces located on the south-east slope outside of the Kanas moraine complex, and at higher elevations (Fig. 1C), are evidence for older glaciation(s). The moraine ridges are oriented roughly parallel to Kanas Valley and we interpret them as lateral moraines, although no terminal moraine in association with these ridges could be unambiguously identified further down the valley.

Kanas Valley glacial chronology

Nine boulders were sampled for cosmogenic exposure dating across the Kanas complex, from three different locations (Fig. 1C). Of the nine ^{10}Be ages obtained, six ages cluster between 18.7 and 22.4 ka (CV, $\sigma/\mu = 8\%$); two are significantly older (48.1 ± 2.7 and 245.4 ± 14.2 ka) and one is significantly younger (11.9 ± 0.7 ka) (Figs 1C and 2; Table 2). For all samples, the ^{26}Al and ^{10}Be ages agree within external uncertainties and hence do not reveal extended periods of burial (Ivy-Ochs and Briner, 2014; Fig. 2; Table 2). The large difference (>100% and >10 ka) between the two oldest ages and the rest of the population probably indicates inheritance (Dortch *et al.*, 2013; Shakun *et al.*, 2015). The youngest sample (11.9 ± 0.7 ka) is from the distal hummocky terrain and might have been exhumed some thousands of years after glacier retreat because of long-lasting ice decay processes (Zech *et al.*, 2005b). Boulder exposure age datasets with wide age spreads, where some ages are significantly affected by inheritance and post-depositional processes, are relatively common for moraine deposits (e.g. Dortch *et al.*, 2013; Heyman, 2014; Blomdin *et al.*, 2016b). After exclusion of these three outliers, the remaining ^{10}Be ages ($n = 6$) indicate that ice retreat from the Kanas complex occurred between ~18 and 22 ka. We also note that these six ^{10}Be ages seem to consist of two populations which correspond to samples collected from the inner part ($n = 3$, mean 19.1 ± 0.4 ka) and from the middle to outer part ($n = 3$, mean 21.8 ± 0.5 ka) of the complex (Figs 1C and 2). We speculate that these populations may reflect successive advances associated with ice margin oscillations during the MIS 2 glaciation.

Single grain IRSL measurements of two samples collected from unsorted, matrix-supported sediment within the Kanas moraine complex (KO13-02 and KAN14-05; Figs 1C and S2, and Table S1) result in widely spread D_e distributions, with overdispersion (OD) values (Galbraith and Roberts, 2012) of 47 and 43%, and skewed or multimodal shapes (Table 3; Figs 3A, C,E and S4). These OD values are significantly larger than values reported in the literature for well-bleached

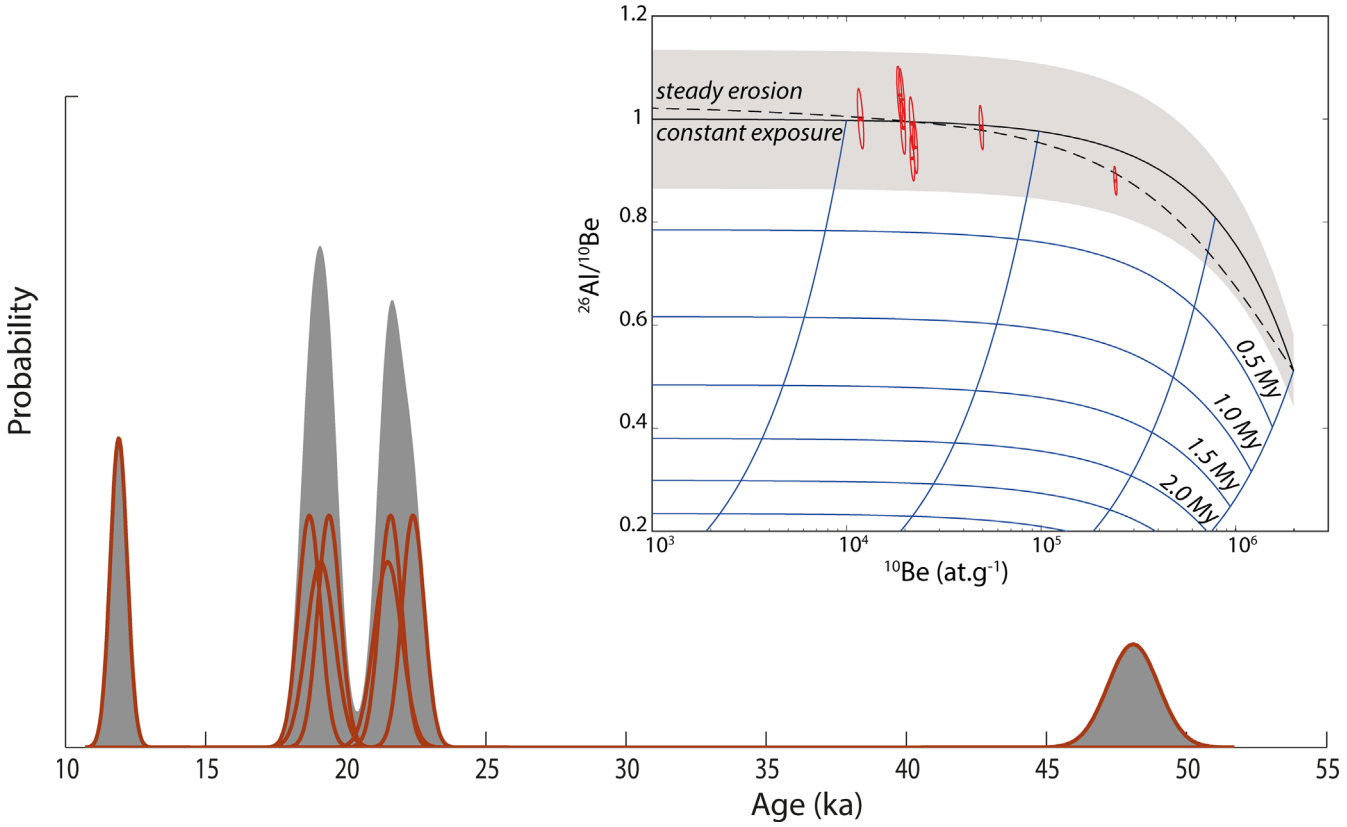

Figure 2. Probability density plot (grey-shaded area) of ^{10}Be exposure ages (individual ages with internal uncertainty are shown with red lines) from the Kanas moraine complex. The oldest ^{10}Be exposure age obtained from the Kanas complex (KC13-27, 245.4 ± 14.2 ka) is located outside the frame. The inset shows the burial plot for the Kanas complex samples. All the concentrations (^{10}Be and ^{26}Al) have been normalized to the long-term average local production rates for each isotope. The blue sub-vertical lines are the burial trajectories for the normalized ^{10}Be concentrations after 10^4, 10^5, 10^6 and 10^7 years of full simple exposure, and the blue sub-horizontal lines represent the full burial times in millions of years (My). The grey area represents the uncertainty for the simple exposure line including the uncertainty for both ^{10}Be and ^{26}Al production rates. The ^{26}Al/^{10}Be ratios do not reveal a significant burial period for any of the samples.

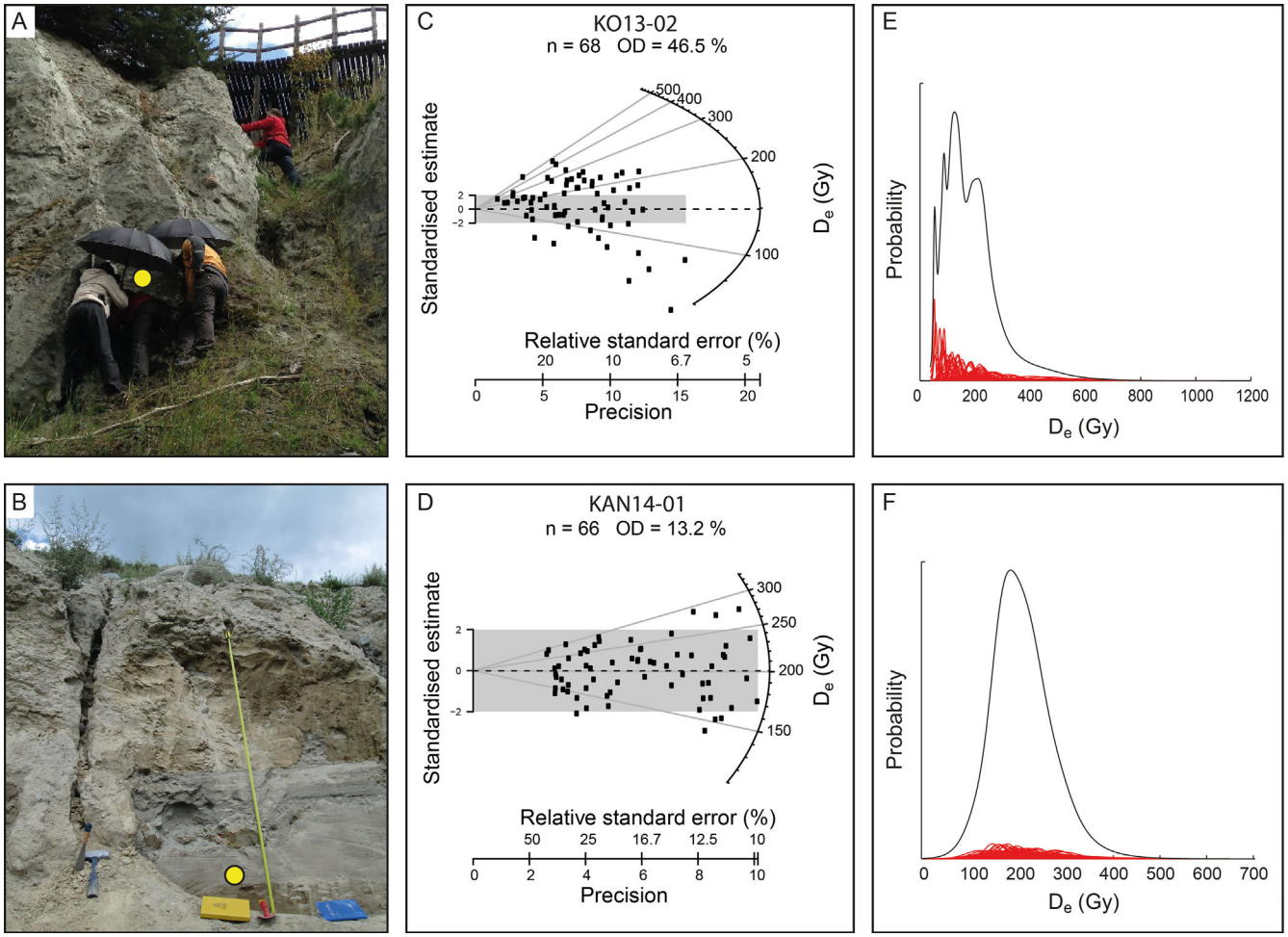

Figure 3. Photographs of the sedimentary sections (A, B), radial plots of measured single grain D_e values (C, D) and probability density distributions (E, F) for one sample interpreted as partially bleached (top, KO13-02, collected within the Kanas moraine complex) and one sample interpreted as well-bleached (bottom, KAN14-01, collected within the outer lateral moraine) before deposition.

glacio-fluvial sediments (~30%, Gaar *et al.*, Figure 3). Taken together with their asymmetrical distributions, the OD values indicate that the Kanas complex samples were incompletely bleached before deposition (Duller, 2008; Bateman *et al.*, 2015). This is further supported by the large differences observed between the CAM fading-corrected ages obtained from single grain and large multi-grain aliquots (fine fraction), with the latter systematically exhibiting older ages (Table 3; cf. Arnold *et al.*, 2012). For a final age determination, identified partial bleaching calls for the application of the MAM. Final fading-corrected MAM single grain IRSL ages indicate a deposition time of the Kanas moraine complex between 23.5 ± 6.1 and 27.4 ± 4.9 ka (Fig. 1C; Table 3). These ages agree within uncertainty with the cosmogenic exposure ages (Fig. 4). Taken together, the cosmogenic and luminescence ages strongly indicate that the Kanas moraine complex was formed during a single MIS 2 glaciation (Fig. 4).

An additional IRSL age of 43.8 ± 6.6 ka (KO13-03), for which no significant partial bleaching effect could be identified, was obtained from a well-stratified glaciofluvial deposit downstream of the Kanas complex (Figs 1C and S2), characterized by horizontal to cross-bedded and sorted to well-sorted layers of sand, gravel, rounded pebbles and cobbles. This age is significantly older than the MIS 2 timing indicated by the OSL and cosmogenic exposure samples collected directly from the Kanas complex itself. However, the sample was collected from a sand layer located ~3 m below the current outwash plain surface and sedimentological characteristics do not permit us to determine if it was originally deposited in a proximal (10^1–10^2 m) or a more distal (10^2–10^4 m) setting relative to a former ice margin (Stephenson et al., 1998; Zielinski and van Loon, 2002). Therefore, this age cannot unambiguously be associated with the Kanas complex ice margin position. Because of the much older age, we hypothesize that the glaciofluvial unit sampled may have been deposited from meltwater from a glacier located further up-valley, and thus older than the Kanas moraine complex. Altogether, we conclude that the age obtained from this sample cannot be used to pinpoint the timing associated with a particular glacial extent, and nor can we determine what the state of the glacier was at the deposition time of the sampled glaciofluvial unit (e.g. retreating or advancing phase). Similar conclusions were drawn by Yang *et al.* (2017), who regarded the dating of glaciofluvial terraces downstream from the Kanas complex unsuitable to identify a glaciation.

Three boulders were collected from the outer lateral moraine ridge located on the south-east slope outside of the Kanas complex, at around 1650 m. a.s.l. (Fig. 1C; Table 2). Two boulders yield similar ^{10}Be ages (63.4 ± 3.5 and 69.0 ± 3.8 ka) while a third has a much younger age (17.2 ± 1.1 ka). The latter age is stratigraphically inconsistent with its geomorphic setting and probably indicates post-depositional reworking. The two older boulders seem to indicate an MIS 4 glaciation, although the limited number of samples ($n = 2$) prohibits any conclusive interpretation based on the cosmogenic exposure age dating alone.

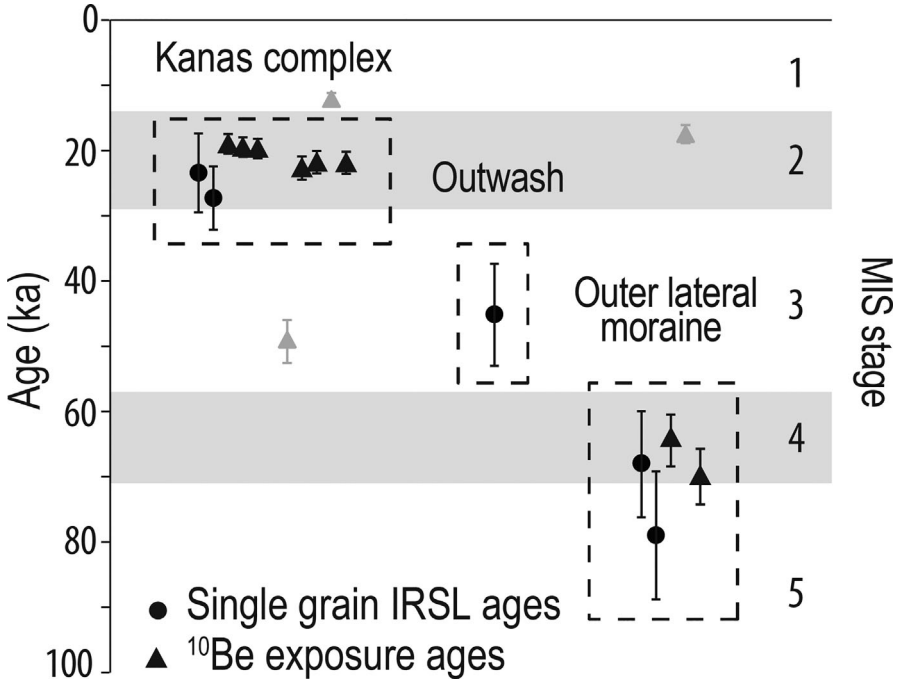

Figure 4. Plot of ^{10}Be exposure and single grain IRSL ages from the Kanas complex, outwash and outer lateral moraine in Kanas Valley. The dashed boxes enclose samples from the same glacial or glaciofluvial landform. Age symbols in grey are outliers and were rejected from landform age determination. The oldest ^{10}Be exposure age obtained from the Kanas complex (KC13-27, 245.4 ± 14.2 ka) is located outside the frame.

Two samples for IRSL dating were collected from glaciofluvial layers incorporated within the same moraine landform located on the south-east slope outside of the Kanas complex (KAN14-01 and KAN14-04; Figs 1C and S2). The coarse single grain D_e distributions show limited overdispersion (13 and 9%, respectively) and symmetric dispersion (Table 3; Figs 3B, D,F and S4), suggesting that the samples were well bleached before deposition. Final fading-corrected CAM single grain IRSL ages are at 68.6 ± 8.2 ka (KAN14-01) and 79.6 ± 9.9 ka (KAN14-04, Table 3) and agree with the two older cosmogenic exposure ages (Fig. 4). A similar time scale is also indicated from luminescence measurements conducted on the fine fraction (68.9 ± 10.5 ka, KAN14-01 and 60.4 ± 9.5 ka, KAN14-04). At this stage, combined IRSL and cosmogenic exposure ages imply the occurrence of a major glacial expansion sometime between ~80 and ~60 ka, during the late MIS 5/MIS 4.

Discussion

Increasing confidence in glacial chronologies using multiple dating methods

Samples collected for cosmogenic exposure and OSL dating across the Kanas moraine complex resulted in six out of nine ^{10}Be exposure ages tightly clustered between ~18 and ~22 ka, and two IRSL ages measured at the single grain scale (>400 grains measured each) of about 25 ka. Samples from the outer lateral moraine (~200 m above the Kanas complex) yield two similar ^{10}Be ages around 65 ka, and two single grain IRSL ages (~200 grains measured each) around 75 ka. In both cases, IRSL and cosmogenic ages agree within error (Fig. 4), supporting MIS 2 and late MIS 5/MIS 4 glaciations in association with each glacial landform sampled. Within this agreement, the luminescence ages tend to be systematically older than the cosmogenic ages. This difference, admittedly within errors, may reflect some systematic uncertainties. First, we assumed no erosion, and it is likely that there is some, which would increase our ^{10}Be exposure ages. This is especially the case for exposure ages from the outer lateral moraine, which could increase by up to 10 ka, based on reported local erosion rates (up to 3 mm ka^{-1}; Koppes *et al.*, 2008; Rother *et al.*, 2014) and the time scale considered. Second, boulders sampled for cosmogenic nuclides may have been shielded by snow, vegetation or even sediment and therefore yield an underestimation of the true age of deposition. Third, laboratory fading rate estimates may include an artificial component (e.g. Lowick *et al.*, 2012), leading to overestimated IRSL ages after fading corrections. Finally, IRSL samples are collected within the body of the moraine landforms, while boulder samples for cosmogenic dating are collected on the surface (representing the very end of active moraine formation) and so might be expected to be younger. Our dataset cannot resolve these potential sources of uncertainty, but as techniques improve these may become less significant. These potential difficulties notwithstanding, our chronology appears robust.

Comparison with previous chronological interpretations

The consistent ^{10}Be exposure and single grain IRSL ages presented here lead to an interpretation of the Kanas complex as reflecting ice margin oscillations within MIS 2, contrasting with previous studies by Xu *et al.* (2009) and Zhao *et al.* (2013) who concluded that the complex was formed during multiple glaciations (MIS 2, 3 and 3/4), based on luminescence dating. The sedimentary unit dated to 34.4 ± 4.2 and 38.1 ± 4.5 ka by Xu *et al.* (2009) was resampled in this study and produced a significantly younger single grain IRSL age of 23.5 ± 6.1 ka. We also obtained another younger single grain IRSL age of 27.4 ± 4.9 ka from a section with similar sedimentological characteristics, but located further downstream in the complex (Fig. 1C). Partial bleaching is known to be common in glacial sediments, as sand grains are typically transported over short distances in turbid water or even subglacially (Duller, 2006; Fuchs and Owen, 2008; Alexanderson and Murray, 2012). If partial bleaching is not detected and accounted for, it results in age overestimation, because the residual signal present at deposition is combined with the dose accumulated since burial. Luminescence measurements of partially bleached samples carried out at the single grain level will result in largely dispersed and asymmetrical D_e

populations (as observed in our measurements), reflecting varying grain depositional histories. In such cases, extraction of the well-bleached sub-population by statistical sampling techniques such as the MAM allows a more accurate estimation of the age of deposition (Duller, 2008; Arnold *et al.*, 2012). However, the typical partial bleaching D_e distribution signature is decreasingly visible with an increasing number of grains measured simultaneously, due to averaging effects (Duller, 2008; Arnold *et al.*, 2012). In Xu *et al.* (2009) and Zhao *et al.* (2013), the OSL signal was measured from the silt fraction (<63 μm) spread on ~10-mm-diameter sample holders, and thus there was averaging of signals emitted by 10^4–10^6 grains. With such a large number of grains, any D_e variability will probably have been masked (Wallinga, 2002; Duller, 2008) and so partial bleaching remained undetected, leading to luminescence age overestimates.

Based on elevation and landform description, the outer lateral moraine ridge dated in this study appears to correspond to the so-called 'fourth moraine complex' identified by Zhao *et al.* (2013), and that the authors connect with MIS 6 ESR ages. The time of deposition determined from our new ^{10}Be and IRSL ages (~60–80 ka) indicates a significantly younger glacial event. ESR dating of glacial deposits remains controversial due to the uncertainty of signal resetting before deposition. Signal accumulated by Ge paramagnetic centers in quartz grains has generally been used for ESR dating of glacial sediments in Central Asia (e.g. Zhou *et al.*, 2002; Zhao *et al.*, 2010). To justify the use of ESR to date glacial sediments, it has been argued that light exposure and grinding during subglacial transport efficiently reset the Ge signal (Yi *et al.*, 2002). However, in several cases when glacial deposits have been dated by both ESR and ^{10}Be exposure techniques, ESR ages were older than ^{10}Be ages, with time differences up to several tens of thousands of years (e.g. Li *et al.*, 2011; Fu *et al.*, 2013). Furthermore, a recent study by Yi *et al.* (2016) that tested the efficiency of light exposure and grinding processes on ESR signal resetting showed that not more than half of the initial Ge signal is reset by grinding processes, and that several days of light exposure would be necessary for a full zeroing of the pre-existing ESR signal. Existing ESR ages from glacial sedimentary deposits should therefore be regarded as age maxima as long as the residual dose cannot be estimated (Yi *et al.*, 2016). Although there are some uncertainties regarding the specific location of the ESR samples, we consider that the apparent discrepancy between the ESR MIS 6 ages (Zhao *et al.*, 2013) and our ^{10}Be-OSL MIS 5/4 ages for the outer lateral moraine above the Kanas complex may be explained by the incomplete ESR signal resetting before deposition. Our new chronology instead appears to match with the MIS 5 timing deduced by Yang *et al.* (2017), based on a stratigraphically older glaciofluvial terrace dated to MIS 6 and a younger lateral moraine ridge tentatively assigned to MIS 4 using OSL dating. However, the OSL samples from the latter study had not been checked for potential partial bleaching and in the absence of direct numerical dating, this timing was, until now, speculative.

Re-evaluation of existing MIS 3 chronologies in Central Asia

Our detailed case study using multiple dating methods led us to revise the age of the major glacial expansion recorded by the Kanas moraine complex to MIS 2. Likewise, a re-evaluation of glacial chronologies in Central Asia seems warranted. The occurrence of a major MIS 3 glaciation in Central Asia can be tested by re-evaluating and comparing published chronological data associated with proposed MIS 3 glacial advances in this region. Data that have previously been used to argue for MIS 3 glaciation (or to suggest a potential MIS 3 event) were compiled from 26 sites from Central Asian mountain ranges, in addition to the MIS 3 glacial chronology proposed in the Kanas Valley (Fig. 5; Appendix S1). Most of the glacial events have been interpreted as having occurred during MIS 3 (14 sites), and others were attributed to either late MIS 4/early MIS 3 (five sites) or to late MIS 3/early MIS 2 (seven sites). We include these sites in our analysis to evaluate the quality of the data and to potentially determine the time window in which each site belongs, using the criteria described in the Methods section. The results of our analysis are presented in Fig. 5B: sites associated with reliable MIS 3 chronologies are represented by a green dot; those associated with chronological data indicating an MIS 2 or MIS 4 glaciation are represented by a yellow dot; and sites for which the reliability of the chronological data remains ambiguous or is insufficient to infer a glaciation timing are represented by a red dot (a detailed analysis of each site is provided in Appendix S1).

Most of the sites associated with a major MIS 3 glacial advance have been dated using a single technique ($n = 24$). Sites for which only one date was available were regarded as unreliable and are labeled red (sites 8, 10, 11 and 14; Fig. 5B). All published luminescence ages are based on measurements conducted on the silt fraction (<63 μm). Using this fraction produces an undifferentiated signal emitted by at least several thousands of grains because silt grains cannot be separated and are spread out as a coating on the surface of large aliquots. For such samples, partial bleaching cannot be evaluated based on an analysis of the distribution of D_e measurements due to averaging processes (Duller, 2008; Arnold *et al.*, 2012). None of the associated papers report an investigation of partial bleaching using other existing approaches, and so the reliability of the proposed luminescence-based chronologies remains ambiguous, pending further verification by additional analysis or dating methods. At this stage, these ages can therefore only be considered as maxima. In our compilation the corresponding sites are therefore labeled red in Fig. 5B (sites 9, 12, 13 and 22–24). For site 9 (Terek Suu site A), the inferred luminescence age is also supported by one cosmogenic exposure age (Koppes *et al.*, 2008). However, because this is a single sample, the MIS 3 timing, while seemingly strengthened, would still require additional luminescence or cosmogenic nuclide data for verification. There are MIS 3 glaciation interpretations at three sites based on ESR dating (sites 15, 16 and 19). At site 19 (Daxi), a reliable cosmogenic dataset that meets the quality criteria described in our Methods section is available (Li *et al.*, 2011), although it indicates an MIS 2 timing (and is labeled yellow in Fig. 5B). For the two other sites the age designation is based on ESR alone, and is thus shown as red in Fig. 5B because ESR ages are considered maximum limiting estimates. Most of the inferred MIS 3 glacial advances in Central Asia are based solely on cosmogenic exposure dating ($n = 19$ sites). Despite the generous approach adopted here that accepts rather small groups of samples as reliable ($n \geq 3$), as long as they also meet moderate clustering requirements ($\sigma/\mu < 15\%$), 15 of the 19 cosmogenic exposure age datasets fail our criteria, and are labeled as red in Fig. 5B. For site 26 (Hangai Dome), only two dates were available and, although these samples agree within internal uncertainty, additional chronological data are required to confirm this strong MIS 3 candidate (Small *et al.*, 2017). In 10 cases (sites 1, 2, 3, 5, 7, 17, 18, 25, 27 and 28), MIS 3 inferences are based on ages that spread evenly over several tens of thousands of years, and often across several marine oxygen

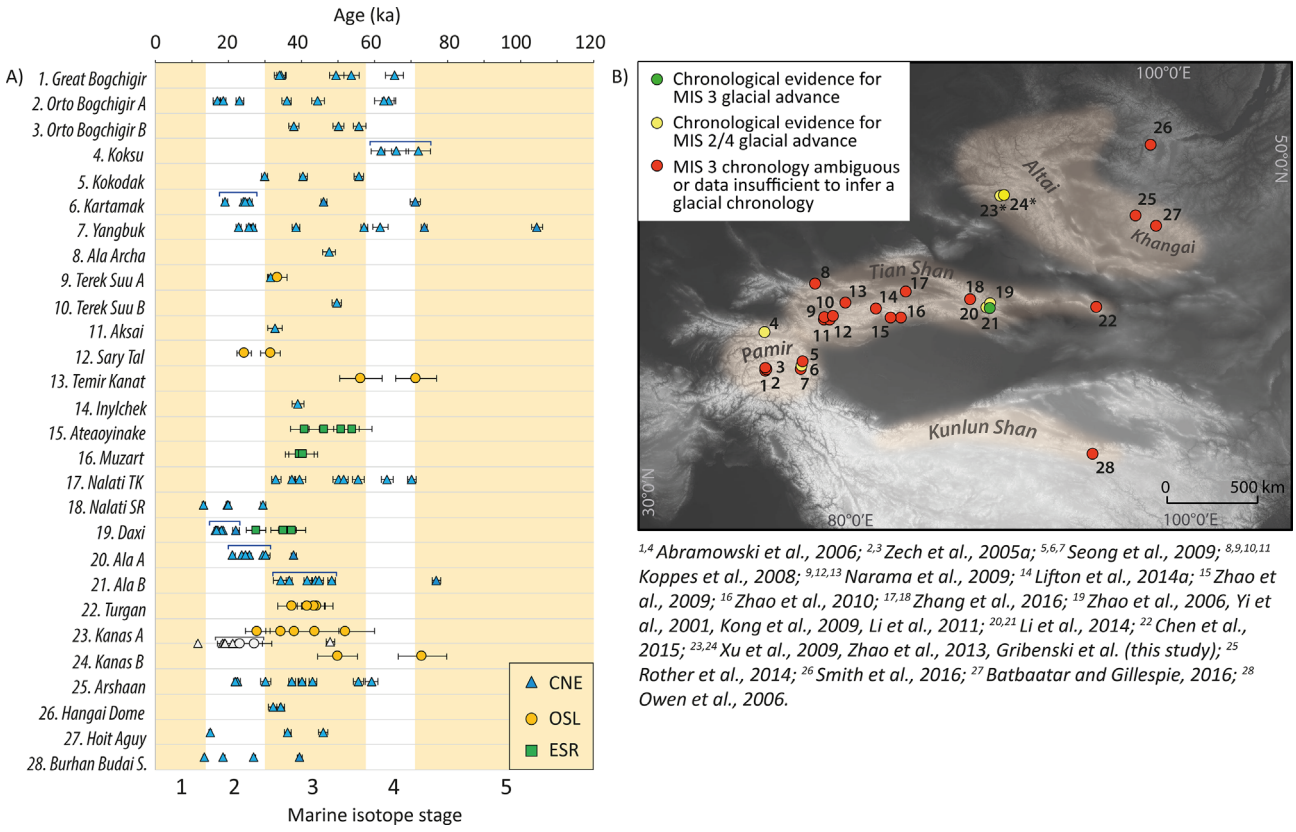

[1,4] Abramowski et al., 2006; [2,3] Zech et al., 2005a; [5,6,7] Seong et al., 2009; [8,9,10,11] Koppes et al., 2008; [9,12,13] Narama et al., 2009; [14] Lifton et al., 2014a; [15] Zhao et al., 2009; [16] Zhao et al., 2010; [17,18] Zhang et al., 2016; [19] Zhao et al., 2006, Yi et al., 2001, Kong et al., 2009, Li et al., 2011; [20,21] Li et al., 2014; [22] Chen et al., 2015; [23,24] Xu et al., 2009, Zhao et al., 2013, Gribenski et al. (this study); [25] Rother et al., 2014; [26] Smith et al., 2016; [27] Batbaatar and Gillespie, 2016; [28] Owen et al., 2006.

Figure 5. (A) Chronological data set and (B) location of the major MIS 3 glacial advances proposed for Central Asia, based on cosmogenic nuclide exposure, optically stimulated luminescence (OSL) and electron spin resonance (ESR) dating of moraines (for location of the map area, see Fig. 1A). The exposure ages have been recalculated following the methodology applied in this study. In A, the horizontal square brackets indicate groups or sub-groups of cosmogenic ages fulfilling the statistical criteria to allow reliable glaciation timing inference ($n \geq 3$; $\sigma/\mu \leq 15\%$), according to the global analysis performed in this study. In B, the color for each location indicates the robustness of the associated chronological dataset (green and yellow locations have robust datasets of different age, red locations have not). Detailed analysis of each site is provided in the supplementary data. *Sites 23 and 24 refer to two MIS 3 glacial advances associated with the Kanas moraine complex, which has been demonstrated in this study to represent a single MIS 2 glaciation. The cosmogenic and luminescence ages produced from the Kanas complex in this study are represented by the gray filled symbols in A.

isotope stages. Of these, none satisfies our criteria after outlier rejection. Such scattered datasets indicate strong geologic effects, which raises doubts about reliable inferences of glaciation timing (Heyman *et al.*, 2011), and so were labeled in red in Fig. 5B. Only five sites have a moderately scattered dataset suitable for constraining a glacial event chronology (sites 4, 6 and 19–21). Our analysis indicates an MIS 2 ($n = 3$) or MIS 4 ($n = 1$) glaciation for four of these sites (labeled in yellow in Fig. 5B), and only in one case does it support a glaciation within MIS 3 (site 21, Ala B, labeled in green in Fig. 5B). This site is located in the Ala Valley, Chinese eastern Tian Shan, and corresponds to a large lateral moraine deposit, extending more than 10 km downstream from identified MIS 2 moraines (Li *et al.*, 2014). While our criteria differ from those of Dortch *et al.* (2013), our results are qualitatively consistent; taken together the cosmogenic nuclide data available at present, as well as the OSL and ESR data, are not consistent with previous notions of large-scale glaciation in Central Asia during MIS 3.

Conclusions

The proposed revised glacial chronology of the Kanas Valley highlights both the opportunities and the difficulties encountered in cosmogenic exposure and luminescence dating of glacial deposits. A limited number of samples, the use of data strongly affected by geomorphological processes (cosmogenic nuclide exposure dating), or the absence of partial bleaching investigations (OSL and ESR) can lead to glacial chronologies that remain tentative. In the Kanas Valley, combined application of cosmogenic dating and single grain luminescence resulted in a re-interpretation of deposits formerly classified as MIS 3 as being MIS 2 in age, and interpretation of a larger glacial advance as late MIS 5/MIS 4 in age. Re-analysis of published chronological data associated with an inferred major MIS 3 glacial advance at 26 additional sites across Central Asia shows that in most cases the data available now do not present a compelling case for a widespread MIS 3 glaciation. However, the chronological data covering this large region are sparse and future studies will undoubtedly provide tighter chronological constraints on Late Pleistocene glacial activity in Central Asia. In particular, combining multiple dating techniques may be a powerful approach to determine the age of pre-LGM deposits with a reasonable degree of confidence.

Supporting Information

Additional supporting information may be found in the online version of this article:

Fig. S1. Boulders sampled in the Kanas Valley for cosmogenic nuclide exposure dating.

Fig. S2. Location and picture of the sedimentary sections sampled for luminescence dating in the Kanas Valley.

Fi. S3. Single grain IRSL D_e values plotted against signal intensity for the sample KAN14-04.

Fig. S4. IRSL single grain D_e distribution associated with the samples collected in the Kanas Valley.

Table S1. Sedimentological description of luminescence samples.

Appendix S1. Re-evaluation of existing MIS3 glacial chronologies in Central Asia: description and detailed chronological data analysis for each site.

Acknowledgements. This work was supported by Swedish Research Council grants to Krister Jansson (No. 2009-4411) and Arjen Stroeven (No. 2011-4892) and Swedish Society for Anthropology and Geography stipend to Natacha Gribenski. Marc Caffee and Nathaniel Lifton acknowledge support from the US National Science Foundation grant EAR-1153689. We are grateful to Fu and Helen for their help in the field, and to Tom Clifton and Greg Chmiel (PRIME Lab) and Sally Lowick (University of Bern) for their support during sample processing. We are also thankful to Sumiko Tsukamoto, Jason Dortch and Bradley Goodfellow and two anonymous reviewers for their valuable suggestions.

References

Abramowski U, Bergau A, Seebach D *et al.* 2006. Pleistocene glaciations of Central Asia: results from ^{10}Be surface exposure ages of erratic boulders from the Pamir (Tajikistan), and the Alay–Turkestan Range (Kyrgyzstan). *Quaternary Science Reviews* **25**: 1080–1096.

Alexanderson H, Murray AS. 2012. Luminescence signals from modern sediments in a glaciated bay, NW Svalbard. *Quaternary Geochronology* **10**: 250–256.

Arnold LJ, Demuro M, Ruiz MN. 2012. Empirical insights into multi-grain averaging effects from 'pseudo' single-grain OSL measurements. *Radiation Measurements* **47**: 652–658.

Auclair M, Lamothe M, Huot S. 2003. Measurement of anomalous fading for feldspar IRSL using SAR. *Radiation Measurements* **37**: 487–492.

Balco G. 2011. Contributions and unrealized potential contributions of cosmogenic-nuclide exposure dating to glacier chronology, 1990–2010. *Quaternary Science Reviews* **30**: 3–27.

Balco G, Stone JO, Lifton NA *et al.* 2008. A complete and easily accessible means of calculating surface exposure ages or erosion rates from ^{10}Be and ^{26}Al measurements. *Quaternary Geochronology* **3**: 174–195.

Batbaatar J, Gillespie AR. 2016. Outburst floods of the Maly Yenisei. Part II – New age constraints from Darhad basin. *International Geology Review* **58**: 1753–1779.

Bateman MD, Evans DJA, Buckland PC *et al.* 2015. Last glacial dynamics of the Vale of York and North Sea lobes of the British and Irish Ice Sheet. *Proceedings of the Geologists' Association* **126**: 712–730.

Benn DI, Evans DJA. 2010. *Glaciers and Glaciation*, 2nd edn. Arnold: London.

Benn DI, Owen LA. 2002. Himalayan glacial sedimentary environments: a framework for reconstructing and dating the former extent of glaciers in high mountains. *Quaternary International* **97–98**: 3–25.

Blair MW, Yukihara EG, McKeever SWS. 2005. Experiences with single-aliquot OSL procedures using coarse-grain feldspars. *Radiation Measurements* **39**: 361–374.

Blomdin R, Heyman J, Stroeven AP *et al.* 2016a. Glacial geomorphology of the Altai and Western Sayan Mountains, Central Asia. *Journal of Maps* **12**: 123–136.

Blomdin R, Stroeven AP, Harbor JM *et al.* 2016b. Evaluating the timing of former glacier expansions in the Tian Shan: a key step towards robust spatial correlations. *Quaternary Science Reviews* **153**: 78–96.

Bøtter-Jensen L, Andersen CE, Duller GAT *et al.* 2003. Developments in radiation, stimulation and observation facilities in luminescence measurements. *Radiation Measurements* **37**: 535–541.

Chen Y, Li Y, Wang Y *et al.* 2015. Late Quaternary glacial history of the Karlik Range, easternmost Tian Shan, derived from ^{10}Be surface exposure and optically stimulated luminescence datings. *Quaternary Science Reviews* **115**: 17–27.

Dortch JM, Owen LA, Caffee MW. 2013. Timing and climatic drivers for glaciation across semi-arid western Himalayan–Tibetan orogen. *Quaternary Science Reviews* **78**: 188–208.

Duller GAT. 2006. Single grain optical dating of glacigenic deposits. *Quaternary Geochronology* **1**: 296–304.

Duller GAT. 2008. Single-grain optical dating of Quaternary sediments: why aliquot size matters in luminescence dating. *Boreas* **37**: 589–612.

Ehlers J, Gibbard PL, Hughes PD, eds. 2011. Quaternary Glaciations – Extent and chronology: a closer Look. *Developments in Quaternary Science, 15*. Elsevier: Amsterdam.

Fu P, Stroeven AP, Harbor JM *et al.* 2013. Paleoglaciation of Shaluli Shan, southeastern Tibetan Plateau. *Quaternary Science Reviews* **64**: 121–135.

Fuchs M, Owen LA. 2008. Luminescence dating of glacial and associated sediments: review, recommendations and future directions. *Boreas* **37**: 636–659.

Gaar D, Lowick SE, Preusser F. 2013. Performance of different luminescence approaches for the dating of known-age glaciofluvial deposits from northern Switzerland. *Geochronometria* **41**: 65–80.

Galbraith RF, Roberts RG. 2012. Statistical aspects of equivalent dose and error calculation and display in OSL dating: an overview and some recommendations. *Quaternary Geochronology* **11**: 1–27.

Galbraith RF, Roberts RG, Laslett GM *et al.* 1999. Optical dating of single and multiple grains of quartz from Jinmium rock shelter, northern Australia: Part I, Experimental design and statistical models. *Archaeometry* **41**: 339–364.

Gribenski N, Jansson KN, Lukas S *et al.* 2016. Complex patterns of glacier advances during the late glacial in the Chagan Uzun Valley, Russian Altai. *Quaternary Science Reviews* **149**: 288–305.

Heyman J. 2014. Paleoglaciation of the Tibetan Plateau and surrounding mountains based on exposure ages and ELA depression estimates. *Quaternary Science Reviews* **91**: 30–41.

Heyman J, Hättestrand C, Stroeven AP. 2008. Glacial geomorphology of the Bayan Har sector of the NE Tibetan Plateau. *Journal of Maps* **4**: 42–62.

Heyman J, Stroeven AP, Harbor JM *et al.* 2011. Too young or too old: evaluating cosmogenic exposure dating based on an analysis of compiled boulder exposure ages. *Earth and Planetary Science Letters* **302**: 71–80.

Hughes ALC, Gyllencreutz R, Lohne ØS *et al.* 2016. The last Eurasian ice sheets – a chronological database and time-slice reconstruction, DATED-1. *Boreas* **45**: 1–45.

Hughes PD, Gibbard PL, Ehlers J. 2013. Timing of glaciation during the last glacial cycle: evaluating the concept of a global 'Last Glacial Maximum' (LGM). *Earth-Science Reviews* **125**: 171–198.

Huntley DJ, Baril MR. 1997. The K content of the K-feldspars being measured in optical dating or in thermoluminescence dating. *Ancient TL* **15**: 11–13.

Huntley DJ, Lamothe M. 2001. Ubiquity of anomalous fading in K-feldspars and the measurement and correction for it in optical dating. *Canadian Journal of Earth Sciences* **38**: 1093–1106.

Ivy-Ochs S, Briner JP. 2014. Dating disappearing ice with cosmogenic nuclides. *Elements* **10**: 351–356.

Kars RH, Reimann T, Ankjaergaard C *et al.* 2014. Bleaching of the post-IR IRSL signal: new insights for feldspar luminescence dating. *Boreas* **43**: 780–791.

Kohl CP, Nishiizumi K. 1992. Chemical isolation of quartz for measurement of in-situ -produced cosmogenic nuclides. *Geochimica et Cosmochimica Acta* **56**: 3583–3587.

Kong P, Fink D, Na C *et al.* 2009. Late Quaternary glaciation of the Tianshan, Central Asia, using cosmogenic ^{10}Be surface exposure dating. *Quaternary Research* **72**: 229–233.

Koppes M, Gillespie AR, Burke RM *et al.* 2008. Late Quaternary glaciation in the Kyrgyz Tien Shan. *Quaternary Science Reviews* **27**: 846–866.

Kuhlemann J, Rohling EJ, Krumrei I *et al.* 2008. Regional synthesis of Mediterranean atmospheric circulation during the Last Glacial Maximum. *Science* **321**: 1338–1340.

Lambeck K, Rouby H, Purcell A *et al.* 2014. Sea level and global ice volumes from the Last Glacial Maximum to the Holocene. *Proceedings of the National Academy of Sciences USA* **111**: 15296–15303.

Li Y, Liu G, Chen Y *et al.* 2014. Timing and extent of Quaternary glaciations in the Tianger Range, eastern Tian Shan, China, investigated using ^{10}Be surface exposure dating. *Quaternary Science Reviews* **98**: 7–23.

Li YK, Liu GN, Kong P *et al.* 2011. Cosmogenic nuclide constraints on glacial chronology in the source area of the Urumqi River, Tian Shan, China. *Journal of Quaternary Science* **26**: 297–304.

Lifton N, Beel C, Hättestrand C *et al.* 2014a. Constraints on the late Quaternary glacial history of the Inylchek and Sary-Dzaz valleys from in situ cosmogenic ^{10}Be and ^{26}Al, eastern Kyrgyz Tian Shan. *Quaternary Science Reviews* **101**: 77–90.

Lifton N, Sato T, Dunai TJ. 2014b. Scaling in situ cosmogenic nuclide production rates using analytical approximations to atmospheric cosmic-ray fluxes. *Earth and Planetary Science Letters* **386**: 149–160.

Lisiecki LE, Raymo ME. 2005. A Pliocene-Pleistocene stack of 57 globally distributed benthic δ 18 O records. *Paleoceanography* **20**: DOI: 10.1029/2004PA001071.

Lowick SE, Trauerstein M, Preusser F. 2012. Testing the application of post IR-IRSL dating to fine grain waterlain sediments. *Quaternary Geochronology* **8**: 33–40.

Narama C, Kondo R, Tsukamoto S *et al.* 2009. Timing of glacier expansion during the Last Glacial in the inner Tien Shan, Kyrgyz Republic by OSL dating. *Quaternary International* **199**: 147–156.

Nishiizumi K. 2004. Preparation of ^{26}Al AMS standards. *Nuclear Instruments and Methods in Physics Research Section B: Beam Interactions with Materials and Atoms* **223–224**: 388–392.

Nishiizumi K, Imamura M, Caffee MW *et al.* 2007. Absolute calibration of ^{10}Be AMS standards. *Nuclear Instruments and Methods in Physics Research Section B: Beam Interactions with Materials and Atoms* **258**: 403–413.

Ochs M, Ivy-Ochs S. 1997. The chemical behavior of Be, Al, Fe, Ca and Mg during AMS target preparation from terrestrial silicates modeled with chemical speciation calculations. *Nuclear Instruments and Methods in Physics Research Section B: Beam Interactions with Materials and Atoms* **123**: 235–240.

Owen LA, Dortch JM. 2014. Nature and timing of Quaternary glaciation in the Himalayan–Tibetan orogen. *Quaternary Science Reviews* **88**: 14–54.

Owen LA, Finkel RC, Haizhou M *et al.* 2006. Late Quaternary landscape evolution in the Kunlun Mountains and Qaidam Basin, Northern Tibet: A framework for examining the links between glaciation, lake level changes and alluvial fan formation. *Quaternary International* **154–155**: 73–86.

Owen LA, Kamp U, Spencer JQ *et al.* 2002. Timing and style of Late Quaternary glaciation in the eastern Hindu Kush, Chitral, northern Pakistan: a review and revision of the glacial chronology based on new optically stimulated luminescence dating. *Quaternary International* **97–98**: 41–55.

Richter D, Richter A, Dornich K. 2013. Lexsyg – a new system for luminescence research. *Geochronometria* **40**: 1–9.

Rother H, Lehmkuhl F, Fink D *et al.* 2014. Surface exposure dating reveals MIS-3 glacial maximum in the Khangai Mountains of Mongolia. *Quaternary Research* **82**: 297–308.

Seguinot J, Rogozhina I, Stroeven AP *et al.* 2016. Numerical simulations of the Cordilleran ice sheet through the last glacial cycle. *The Cryosphere* **10**: 639–664.

Seong YB, Owen LA, Yi C *et al.* 2009. Quaternary glaciation of Muztag Ata and K Shan: evidence for glacier response to rapid climate changes throughout the Late Glacial and Holocene in westernmost Tibet. *Geological Society of America Bulletin* **121**: 348–365.

Shakun JD, Clark PU, Marcott SA *et al.* 2015. Cosmogenic dating of Late Pleistocene glaciation, southern tropical Andes, Peru. *Journal of Quaternary Science* **30**: 841–847.

Sharma P, Bourgeois M, Elmore D *et al.* 2000. PRIME lab AMS performance, upgrades and research applications. *Nuclear Instruments and Methods in Physics Research Section B: Beam Interactions with Materials and Atoms* **172**: 112–123.

Small D, Clark CD, Chiverrell RC *et al.* 2017. Devising quality assurance procedures for assessment of legacy geochronological data relating to deglaciation of the last British–Irish Ice Sheet. *Earth-Science Reviews* **164**: 232–250.

Smedley RK, Pearce NJG. 2016. Internal U, Th and Rb concentrations of alkali-feldspar grains: implications for luminescence dating. *Quaternary Geochronology* **35**: 16–25.

Smith SG, Wegmann KW, Ancuta LD *et al.* 2016. Paleotopography and erosion rates in the central Hangay Dome, Mongolia: landscape evolution since the mid-Miocene. *Journal of Asian Earth Sciences* **125**: 37–57.

Stephenson DA, Fleming AH, Mickelson DM. 1998. Glacial deposits. In *Hydrogeology*, The Geology of North America; v O-2, Back W, Rosenhein JS, Seaber PR (eds). Geological Society of America: Boulder, CO.

Trauerstein M, Lowick SE, Preusser F *et al.* 2014. Small aliquot and single grain IRSL and post-IR IRSL dating of fluvial and alluvial sediments from the Pativilca valley, Peru. *Quaternary Geochronology* **22**: 163–174.

van Meerbeeck CJ, Renssen H, Roche DM. 2009. How did Marine Isotope Stage 3 and Last Glacial Maximum climates differ? – perspectives from equilibrium simulations. *Climate of the Past* **5**: 33–51.

Wallinga J. 2002. Optically stimulated luminescence dating of fluvial deposits: a review. *Boreas* **31**: 303–322.

Wallinga J, Murray A, Wintle A. 2000. The single-aliquot regenerative-dose (SAR) protocol applied to coarse-grain feldspar. *Radiation Measurements* **32**: 529–533.

Wintle AG, Murray AS. 2006. A review of quartz optically stimulated luminescence characteristics and their relevance in single-aliquot regeneration dating protocols. *Radiation Measurements* **41**: 369–391.

Xu XK. 2010. *Late Pleistocene glacial geomorphology and dating in Kanas River Valley, Altai mountains*. PhD Thesis, Graduate University of the Chinese Academy of Sciences, Beijing (in Chinese with English abstract).

Xu XK, Yang JQ, Dong GC *et al.* 2009. OSL dating of glacier extent during the Last Glacial and the Kanas Lake basin formation in Kanas River valley, Altai Mountains, China. *Geomorphology* **112**: 306–317.

Yang J, Chen Y, Xu X *et al.* 2017. Quaternary glacial history of the Kanas Valley, Chinese Altai, NW China, constrained by electron spin resonance and optically stimulated luminescence datings. *Journal of Asian Earth Sciences* **147**: 164–177.

Yi C, Bi W, Li J. 2016. ESR dating of glacial moraine deposits: some insights about the resetting of the germanium (Ge) signal measured in quartz. *Quaternary Geochronology* **35**: 69–76.

Yi C, Jiao K, Liu K *et al.* 2001. ESR dating on tills and the last glaciations at the head waters of the Urumqi River, Tianshan Mountains, China. *Journal of Glaciology and Geocryology* **23**: 389–393 (in Chinese with English abstract).

Yi C, Jiao K, Liu K *et al.* 2002. ESR dating of the sediments of the Last Glaciation at the source area of the Urumqi River, Tian Shan Mountains, China. *Quaternary International* **97–98**: 141–146.

Zech R, Abramowski U, Glaser B *et al.* 2005a. Late Quaternary glacial and climate history of the Pamir Mountains derived from cosmogenic ^{10}Be exposure ages. *Quaternary Research* **64**: 212–220.

Zech R, Glaser B, Sosin P *et al.* 2005b. Evidence for long-lasting landform surface instability on hummocky moraines in the Pamir Mountains (Tajikistan) from ^{10}Be surface exposure dating. *Earth and Planetary Science Letters* **237**: 453–461.

Zhang M, Chen Y, Li Y *et al.* 2016. Late Quaternary glacial history of the Nalati Range, central Tian Shan, China, investigated using ^{10}Be surface exposure dating. *Journal of Quaternary Science* **31**: 659–670.

Zhao J, Liu S, He Y *et al.* 2009. Quaternary glacial chronology of the Ateaoyinake River Valley, Tianshan Mountains, China. *Geomorphology* **103**: 276–284.

Zhao J, Song Y, King JW *et al.* 2010. Glacial geomorphology and glacial history of the Muzart River valley, Tianshan Range, China. *Quaternary Science Reviews* **29**: 1453–1463.

Zhao J, Yin X, Harbor JM *et al.* 2013. Quaternary glacial chronology of the Kanas River valley, Altai Mountains, China. *Quaternary International* **311**: 44–53.

Zhao J, Zhou S, He Y *et al.* 2006. ESR dating of glacial tills and glaciations in the Urumqi River headwaters, Tianshan Mountains, China. *Quaternary International* **144**: 61–67.

Zhou S, Li J, Zhang S. 2002. Quaternary glaciation of the Bailang River Valley, Qilian Shan. *Quaternary International* **97–98**: 103–110.

Zielinski T, van Loon AJ. 2002. Present-day sandurs are not representative of the geological records. *Sedimentary Geology* **152**: 1–5.